Analyses of small facets imaged with scanning-probe microscopy

Hegeman, J. B. J. W.; Kooi, B. J.; Groen, H. B.; de Hosson, J. Th. M.

Published in:
Journal of Applied Physics

DOI:
10.1063/1.371275

Analyses of small facets imaged with scanning-probe microscopy

J. B. J. W. Hegeman, B. J. Kooi, H. B. Groen, and J. Th. M. De Hosson[a)]
Department of Applied Physics, Materials Science Centre and Netherlands Institute for Metals Research, University of Groningen, Nijenborgh 4, 9747 AG Groningen, The Netherlands

(Received 25 March 1999; accepted for publication 29 June 1999)

Two tools for the analysis of facets as detected by scanning-probe microscopy (SPM) images are proposed. One tool is an adaptation of the radial-histogram transform proposed by D. Schleef *et al.* in Phys. Rev. B. **55**, 2535 (1997). In this article the local slopes in the SPM image are in the present version determined by Savitsky–Golay filters with variable lengths [A. Savitsky and M. J. E. Golay, Anal. Chem. **36**, 1627 (1964)]. These variable length filters turn out to be important to suppress the influence of noise obscuring the possibility to detect facets and to analyze corrugations with different length scales in SPM images, e.g., surface reconstructions. The other tool allows the direct quantitative determination of the orientation (with a standard deviation) of user-specified parts of facets. It makes use of a Savitsky–Golay filter as well. Both tools were applied to an artificially constructed SPM image and several experimental SFM images showing (ionic) MnO precipitates protruding out of a (metallic) Cu surface. It is shown that the Miller indices of the facets can be derived experimentally. © *1999 American Institute of Physics.* [S0021-8979(99)04919-1]

I. INTRODUCTION

Scanning-probe microscopy (SPM) proved to be a versatile tool to provide quantitative information on surface topography within the length scale ranging from over 100 μm down to atomic sizes. Often tools are needed that translate the general information of the SPM images into the desired specific quantitative information, e.g., roughness parameters [e.g., Refs. 1–8] or faceting of the surface [e.g., Refs. 9–13]. The purpose of the present work is to illustrate the application of two different approaches for the analyses of facets. The first tool is an adaptation of the radial-histogram transform (RHT) as proposed by Schleef *et al.*[14] With this transform the SPM image is converted into a histogram showing the distribution of the relative amount of image area as a function of its surface normal, where the surface normal is described by spherical coordinates. In the original RHT proposed the first derivative of height z with respect to x and y around each pixel with (x,y) position (i,j) is obtained by taking $(z_{i+1,j}-z_{i-1,j})/2$ and $(z_{i,j+1}-z_{i,j-1})/2$, respectively,[14] i.e., the derivative is taken over a length scale of 3 pixels. In the presence of noise and particularly in combination with grazing inclination angles of facets, the ability of this 3-pixel filter to detect facets is rather poor. Further, since facets are characterized by a length scale generally much larger than 3 pixels, also the filter used for determining the first derivative can be taken clearly larger than 3 pixels. An efficient convolution filter for differentiation of data over variable length scales is a filter proposed by A. Savitsky and M. J. E. Golay.[15] So, the RHT proposed in Ref. 14 is adapted here by implementing the Savitsky–Golay filter, thereby reducing the need for a severe smoothing when making the histogram, and also enabling the construction of RHTs for different filter lengths. The importance of this adaptation related to corrugations with different length scales and noise in SPM images will be illustrated by an artificially created SPM image and by several experimental SFM images.

Although the RHT peaks can be identified corresponding to the orientation of facets in space, the direct link between a certain area in the SPM image identified as a facet and the peak in the RHT is lost. Also a list with quantitative data on the peak positions in the RHT is not directly available. Often, it is convenient to determine directly the orientation of facets for user-assigned parts of the image corresponding to the different facets, i.e., perform a direct plane fitting to facets. This is the basis for the second tool considered in this work. The first derivative in this case is also determined by the Savitsky–Golay-type filter, but with lengths of the filter equal to the two sides of the user-specified rectangle centered on a facet in the SPM image.

If crystallographic knowledge of the system under study is available, the orientation of facets and the angles between facets can be translated into the Miller indices of the facets. This procedure has been performed frequently to analyze facets imaged by SPM (see, e.g., Refs. 9–11). However, the orientation of facets and angles between facets was based on single line scans (poor statistics) taken from the image[9,11] or on averaging of line scans.[10] A clear disadvantage is, however, that it is restricted to cases were facets can be contracted to one-dimensional objects. Errors in the determination of angles between facets are easily made using line scans, because the line scans should be taken such that they are lying in the plane formed by the two unknown surface normals of the two facets between which the angles should be determined. The present tools do not have the problems of line scans, because they treat facets as planes with orientations in three-dimensional space.

The experimental examples presented in this work deal with small oxide precipitates in a metal matrix, i.e., MnO precipitates in Cu as obtained by internal oxidation. The Cu/

[a)]Electronic mail: hossonj@phys.rug.nl

MnO interface structure on an atomic scale has previously been characterized by high-resolution transmission electron microscopy (HRTEM).[16–18] Interesting about the interface is that the oxide has a strong preference to terminate with a close-packed oxygen plane which is a polar plane. The general shape of the precipitate is an octahedron bound by eight such close-packed oxide planes parallel to eight close-packed metal planes. The preference for a terminating close-packed polar plane is general for NaCl structure-type oxides in fcc matrix and also observed in other system types.[19–21] The terminating plane at a surface can never be a polar plane having a dipole in the repeat unit perpendicular to the surface, because it is associated with a diverging surface energy.[22] The stability of the polar plane at the interface within the metal is provided by image charges and screening in the metal.[23,24] Due to the strong difference in stability of the polar oxide facets within the metal and at the surface, characterization of the facets for the region where the precipitates make the transition from below to above the surface is of great interest. Within this context the SFM images of the oxide precipitates protruding out of the surface are made.

II. TOOLS FOR ANALYSIS OF FACETS

A. RHT

A thorough description of the RHT is given in Ref. 14. In Eqs. (1) and (2) in this reference the first derivatives of height z with respect to x and y around each pixel with (x,y) position (i,j) are defined as:

$$\left[\frac{\partial z}{\partial x}\right]_{i,j} = \frac{1}{2}[z_{i+1,j} - z_{i-1,j}],$$

$$\left[\frac{\partial z}{\partial y}\right]_{i,j} = \frac{1}{2}[z_{i,j+1} - z_{i,j-1}],$$

where it is assumed that the image is equi-axed; in principle the denominator 2 has to be multiplied by the length per pixel in the SPM image using the same units as for the z scale. The earlier derivative can be conceived as the application of the following convolution filter to the rows and columns of the matrix containing the z_{ij} elements of the SPM image: $[-1\ 0\ 1]/2$.

This 3-points filter is a specific, shortest version of a generic filter for determination of the first derivative of data that is assumed to show linear or quadratic dependence with respect to the spacing of the data elements in an array (e.g., rows or columns in a matrix). This type of filter was proposed by A. Savitsky and M. J. E. Golay, together with smoothing filters and nth derivative filters ($n=1-5$) for data that can be assumed to be either linear functions or polynomial functions up to the 6th degree.[15] The results of these convolution filters are identical to the ones for a linear least-squares fitting procedure, but can be applied very efficiently in computer algorithms. Since for facets we can safely assume that z is a linear function of x or y, the correct filter with a length $2n+1$ with n integer (excluding zero) for taking the first derivative is of the following form:

$$[-n\ -(n-1)\ -(n-2)\cdots -1\ 0\ 1\cdots(n-2)\ (n-1)\ n]/\left(2\sum_{i=1}^{n} i^2\right)$$

This convolution filter for taking the first derivative of the SPM data is in principle the only adaptation made to the RHT as proposed by Schleef *et al.*,[1] but as will be shown later can be of crucial importance. When constructing the histogram, multiple bins H_{kl} are filled by the area A_{ij} of the SPM image in proportion to:

$$H_{kl} = \sum_{i,j} A_{ij} \exp(-\gamma_{kl}^2/\alpha^2)$$

where γ_{kl} is the angular separation between the bin specified by its spherical coordinates (ϕ_k, θ_l) and the surface normal for A_{ij} determined by the differentiation procedure (with conversion in spherical coordinates).[14] The factor α is a smoothing factor. With a 3-points filter in the presence of noise in SPM images, particularly in combination with grazing angles of the facets (where the absolute change in height z over 3 pixels is small), the error in determination of the surface normal can be large. To reduce the consequently introduced noise in the histogram, a relatively large smoothing factor α is needed. Using longer filters (which perform a linear least-squares fit) the error in determining the surface normals is reduced and consequently a smaller smoothing factor can be applied.

Of course, in the absence of noise, most detailed information is obtained by the shortest differentiation filter, because such a filter can follow best sudden changes in surface normals in the SPM image. Long filters smear out abrupt changes. For instance, two facets with different orientation showing an abrupt continuation will after differentiation give the impression that they pass gradually over in each other; the longer the filter the more gradual the transition will appear.

However, also in the absence of noise, filters with different lengths can be of practical use, because they may point at corrugations with different length scales present in the SPM image. For instance, one large facet may reconstruct in an alternating series of two different small facets. Short differentiation filters may indicate the presence of the two different small facets, whereas filters exceeding a certain length give the orientation of the overall large facet, which presence will not be evident at all in the RHT using the short filter only. An artificial SPM image is constructed in order to demonstrate this idea; see Sec. IV A.

B. Direct facet-orientation determination

Facets in SPM images can often be identified directly. Then, one may want to obtain quantitative information on the orientation of these facets. For this purpose the earlier RHT can be used. However, it is merely a transform of the original SPM image and does not directly supply quantitative information on the orientation of a specific facet. Then, an additional routine can be used which identifies the exact quantitative positions of the peaks in the histogram. This is a rather cumbersome procedure if the orientations of specific

facets already identified in the SPM image are wanted. Further, peaks in the histogram are easily assigned to certain facets. However, the direct link to a localized area in the image is lost during construction of the histogram, and therefore, the assignment of a peak in the histogram to a certain image area should be done with care. These two points make clear that a routine in addition to the RHT, which determines directly the orientation of user-specified areas in the SPM image which correspond to the different facets, is desirable. Such a routine is constructed that enables the user to specify, by computer, rectangles in the SPM image. Each rectangle should be drawn as large as possible, but within the extension of the facet to be analyzed. The height data z within the rectangular matrix with size n,m in the x,y-direction is thus considered to represent a straight plane. The surface normal of this plane is the information wanted. The first derivative of z with respect to x is determined m times by applying the earlier defined Savtisky–Golay filter with a length n to the m columns with length n. From these m values the average and standard deviation for the derivative $\partial z/\partial x$ can be obtained readily. Analogously, the first derivative of z with respect to y is determined n times by applying the filter with a length m to the n rows with length m. Using this procedure the orientations of facets as well as the errors in their orientations are determined directly.

III. EXPERIMENT

An alloy of copper containing 1 at. % manganese was prepared in a high-frequency furnace by melting the pure constituents (purity 99.99% by weight) in an alumina crucible under oxygen-free argon protective atmosphere. The ingot was homogenized (1 week 700 °C) and subsequently cold rolled from 4 mm down to 0.5 mm. Oxidation was performed in a Rhines pack[25] (Cu-foil containing Cu, Cu_2O and Al_2O_3 powder in volume ratio of about 1:1:1) at 900 °C (for times ranging from 5 h to 1 week) in an evacuated quartz tube. Using this method MnO precipitates inside Cu were obtained which have a typical size of 300 nm and show predominantly a parallel topotaxy with the Cu matrix. These precipitates have octahedral shape owing to termination of the precipitate by 8 MnO {111} facets.[16–18]

Round 3 mm transmission electron microscopy disks were ground (mesh 1200) and subsequently ion milled several hours using an Ar^+ ion beam of 4 kV under a grazing angle of 13.5° (Gatan dual ion mill model 600). During ion milling the sample was rotated around its surface normal. Subsequently the 3 mm disks were ''glued'' on 15 mm steel disks using wax and a hot plate at a temperature of 130 °C. This procedure of annealing the sample at 130 °C in air after the ion milling appeared to be essential for obtaining the sharp faceting of the MnO precipitates protruding out of the Cu surface.

SFM imaging was performed with a Nanoscope II from Digital Instruments using a $9\times9\,\mu$m (i.e., D) scanner. Height and force images with a size of 400×400 pixels were obtained using gold coated pyramidal silicon nitride tips (Nanoprobe tips from Digital Instruments). Images were taken both in air (Secs. IV B and IV D) and in a commercially available fluid cell from Digital Instruments for Nanoscope II (Sec. IV C). The dissolution of the MnO precipitates at the surface (Sec. IV C) was performed in such a fluid cell by using a mixture of ethanol, water and sodium chloride and by simultaneously scanning (for about 1.5 h). During scanning the faceted etch pits gradually emerged. Ammonium chloride instead of sodium chloride turned out to be too aggressive; MnO was predominantly dissolved, but also Cu was affected.

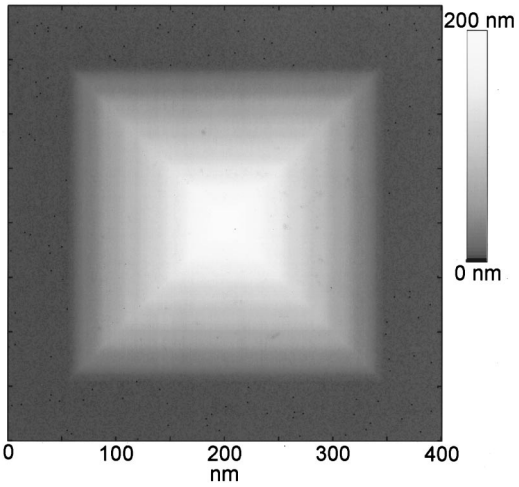

FIG. 1. Artificially constructed SPM height image depicting a faceted MnO precipitate protruding out of a Cu{001} surface. Four large facets corresponding to MnO{111} are readily observable, but each of these large facets are reconstructed into an alternation of two small facets. Noise in the image is present with a normal distribution around zero and a variance of 1 which can be related to the pixel length 1 in the image.

IV. RESULTS AND DISCUSSION

A. Reconstructed octahedron

An artificially constructed SPM image with noise added is shown in Fig. 1. The artificial noise used has a normal distribution probability around zero and in Fig. 1 a variance 1 in (z direction) which can be related to the pixel length (in x and y direction) which is 1. A pyramid protruding out of the surface can be recognized readily in the image. The RHTs for applying Savitsky–Golay filter lengths of 3 and of 20 pixels to this image but with a lower noise level of variance 0.1 are shown in Figs. 2(a) and 2(b) respectively. In Fig. 2(a) for each 90 °ϕ (azimuth) peaks at about 35° and 65 °θ (inclination) are observed. On the other hand, in Fig. 2(b) for the same each 90 °ϕ only one peak (although rather broad in θ) is observed at about 55 °θ. The combined information from Figs. 2(a) and 2(b) indicate that each of the four large facets of the pyramid having an inclination of 55° is reconstructed within a length scale of 20 pixels or smaller into two facets with inclinations of 35° and 65°. From a combination with Fig. 2(a) after careful inspection of the original image, it could be concluded that each of the four large facets is reconstructed into two smaller facets. However, then no quantitative information on the inclination of the large facets is available and the length scale within which the overall facets reconstruct into the smaller ones is also unknown.

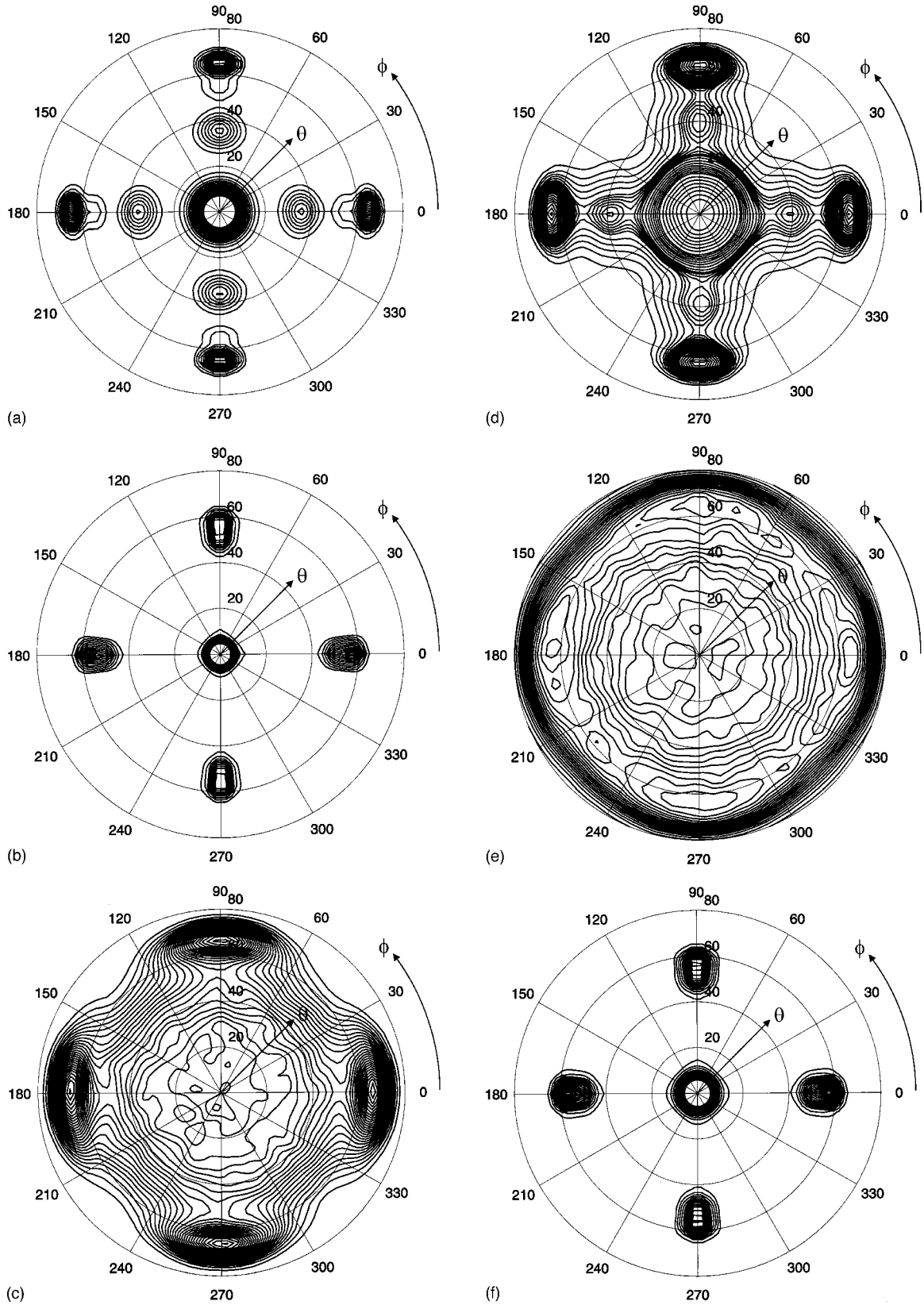

FIG. 2. RHT of the image shown in Fig. 1 with different levels of noise and obtained by using Savitsky–Golay filters with a different pixel lengths for determining the local slopes in the image. (a) Noise having variance 0.1 and a filter length of 3 pixels. The RHT shows for each 90 °ϕ (azimuth) facets at 35 and 65 °θ (inclination). (b) The analogous RHT as in (a) but now constructed using a filter length of 20 instead of 3 pixels. The RHT shows for each 90 °ϕ only a facet at 55 °θ. (c) Noise having variance 0.5 and a filter length of 3 pixels. The RHT shows for each 90 °ϕ only a facet at 65 °θ. The facet at 35 °θ is lost in the noise. (d) The analogous RHT as in (c), but now constructed using a filter length of 5 instead of 3 pixels. The facets at 35 °θ are now recaptured from the noise. (e) Noise having a variance of unity and a filter length of 3 pixels. The RHT indicates for each 90 °ϕ only faintly a facet at 65 °θ. Comparing Figs. (a),(c), and (e) indicates the large influence of noise on detecting facets with a 3-point filter. (f) The analogous RHT as in (e), but now constructed using a filter length of 20 instead of 3 pixels. The RHT shows for each 90 °ϕ clearly a facet at 55 °θ. Comparing Figs. (b) and (f) indicates the small influence of noise on detecting facets with a 20-point filter.

The image in Fig. 1 is not totally hypothetical. With respect to the MnO precipitates in Cu (see later), where both phases have cubic lattices, the fourfold symmetry observed in the image which is also clearly revealed by the RHTs, indicates that the horizontal plane in the image is a cube plane of the pyramid. Then, the observation of four large facets with an inclination angle of $55\,°\theta$ with respect to the horizontal plane makes it probable that {111} type facets are present. To be sure about the type of facets an additional crystallographic direction has to be known. In the examples that will be shown below this information is always available, since it is known from HRTEM that the MnO precipitates within Cu have almost perfect octahedral shape bound by eight {111} planes (and that parallel topotaxy exists between MnO and Cu).[16–18] Then, in principle the circumference made by intersection of an arbitrary surface plane with the octahedron always enables determination of the complete crystallographic orientation of the precipitate protruding out of the surface (although this determination is not always easy; see Sec. IV D).

The image in Fig. 1 was indeed constructed to simulate a MnO octahedron protruding out of the Cu(100) surface. Since the polar {111} facets of MnO are only stable inside the Cu matrix due the screening of the metal, these facets exposed at the surface have to reconstruct in nonpolar facet types (at least not having a dipole moment in the repeat unit perpendicular to the surface).[22] The reconstruction of the {111} facets introduced in the SPM image Fig. 1 is artificial and purely hypothetical.

The RHTs shown in Figs. 2(a) and 2(b) are for the image shown in Fig. 1 but for such a low noise level (variance 0.1) that the 3-point Savtisky–Golay filter is not notably influenced, i.e., the results are similar to the ones for the image without noise. Repeating the RHT for the 3-point filter, but now for an increased noise level having a variance of 0.5 (compared to a pixel length 1) yields the results shown in Fig. 2(c). The effect of noise on the RHT is clearly visible, because the four peaks at an inclination angle θ of 35° have now become undetectable in the RHT. The four peaks at $65\,°\theta$ are still clearly present. Increasing the filter length from 3- to 5-points recaptures the four peaks at 35° from the noise as can be seen in Fig. 2(d). Although the total surface area for facets with $35\,°\theta$ is the same as for facets with $65\,°\theta$ the peak heights at 35° are due to the noise considerably smaller than the ones at 65°. The example shown in Figs. 2(c) and 2(d) clearly indicates the importance of having a variable filter lengths for the detection of facets in SPM images.

Further increasing the noise level to a variance of 1, which is in fact the noise level of the image shown in Fig. 1, gives for the 3- and 20-points filters the RHTs shown in Figs. 2(e) and 2(f), respectively. In Fig. 2(e) for the 3-points filter peaks can hardly be recognized anymore; only four faint peaks for each $90\,°\phi$ at about $65\,°\theta$ are still detectable. On the other hand, in Fig. 2(f) for the 20-points filter the four peaks for each $90\,°\phi$ at about $55\,°\theta$ are still well detectable. Comparing Figs. 2(a) and 2(e) the influence of noise is dramatic, whereas the difference between Figs. 2(b) and 2(f) is not directly observable, indicating that the same noise level hardly affects the results of the 20-points filter.

TABLE I. Orientation and deviation using spherical coordinates in degrees of the facets of the (MnO) pyramid shown in Fig. 1 as obtained by the DFOD.

	Facet 1	Facet 2	Facet 3	Facet 4
Azimuth ϕ	−89.9	−0.1	89.9	180.0
$d\phi$	0.9	0.5	0.2	0.2
Inclination θ	54.7	54.6	54.4	54.5
$d\theta$	0.9	0.5	0.3	0.2

It is clear that at increasing noise the possibility to detect facets at a fixed filter length is obscured at first instance for small inclination angles and gradually becomes obscured for larger angles θ. This obscuring effect is reduced to smaller angles θ if the filter length is increased. In the end it is just simply a matter of the overall change in height over the length of the filter with respect to the random error in height per pixel. The effect of noise will again become significant in the next section dealing with an experimental SFM image.

The results of the direct facet-orientation determination (DFOD) are given in Table I. Without a detailed analysis and in the presence of noise the reconstruction is easily missed and only the four large facets are observed and thus analyzed by the DFOD. The results indicate that the orientation of the four large facets of the pyramid are well reproduced within a few tenths of a degree by the DFOD (with a calculated error that is overestimated), despite the reconstruction and the noise with a variance of 1.0 present. The advantage of this method is the direct available quantitative information, the disadvantage is that only facets are analyzed that are already *a priori* identified.

B. MnO precipitates viewed nearly along ⟨100⟩

A SFM image of two MnO precipitates protruding out of a Cu surface is shown in Fig. 3. Both precipitates clearly

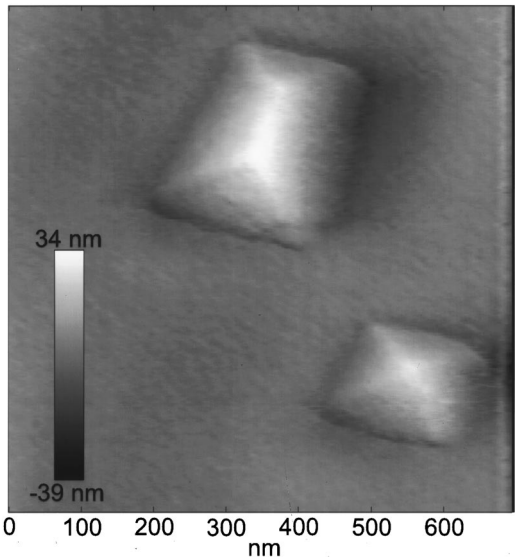

FIG. 3. Experimental SFM height image showing two faceted MnO precipitates protruding out of a Cu surface. The faceting of the two precipitates is identical.

show faceting that is also similar for both precipitates. The quality of the image is far from optimal; compare for instance with the less-noisy images shown in Fig. 7. However, this noise is meaningful, because it will nicely demonstrate the usefulness of applying Savitsky–Golay filters with different lengths for the determination of the derivatives in SPM images as needed for a full characterization of the orientations of facets. From the image with a size of 400 $\times$400 pixels, 200$\times$200 pixels in the center of the upper half, incorporating the image of the bigger one of the two precipitates, are selected for the RHT. The RHT for a filter length of 3 pixels is shown in Fig. 4(a) and for a filter length of 25 pixels is shown in Fig. 4(b). The presence of four facets is clearly revealed by the transform in Fig. 4(b), whereas the transform of Fig. 4(a) does not indicate the presence of any of these facets. Apparently the random error in height associated with the pixels in the image has a magnitude that it is similar to the change of height within 3 pixels of the facets. On the other hand the change of height on a larger length scale (i.e., 25 pixels) is certainly significant and larger than the average error in height per pixel. Therefore, a linear least-squares fit to the data of 25 pixels to determine the derivative reveals the presence of the facets in the transform.

The results of the direct determination of the orientation of the facet are given in Table II. The fourfold symmetry exhibited by the facets in Fig. 3, becoming apparent from the RHT in Fig. 4 and the DFOD results in Table II (i.e., the facets have similar θ and they occur for about each 90 °ϕ), indicate that the surface normal is close to the cube directions of the Cu and MnO. Furthermore, since it is known that the part of the precipitate within the Cu is an octahedron, the circumference of the precipitate caused by the intersection with the Cu surface corresponds to the $\langle 110 \rangle$ directions within the (001) plane. Finally, with the determined polar angle θ of the four facets of 21.7$\pm$1°, the type of facets present can be identified as near to {227} (i.e., the MnO pyramid is bound by the (227), ($\bar{2}27$), ($2\bar{2}7$), and ($\bar{2}\bar{2}7$) facets). As expected these facets correspond to nonpolar MnO planes.

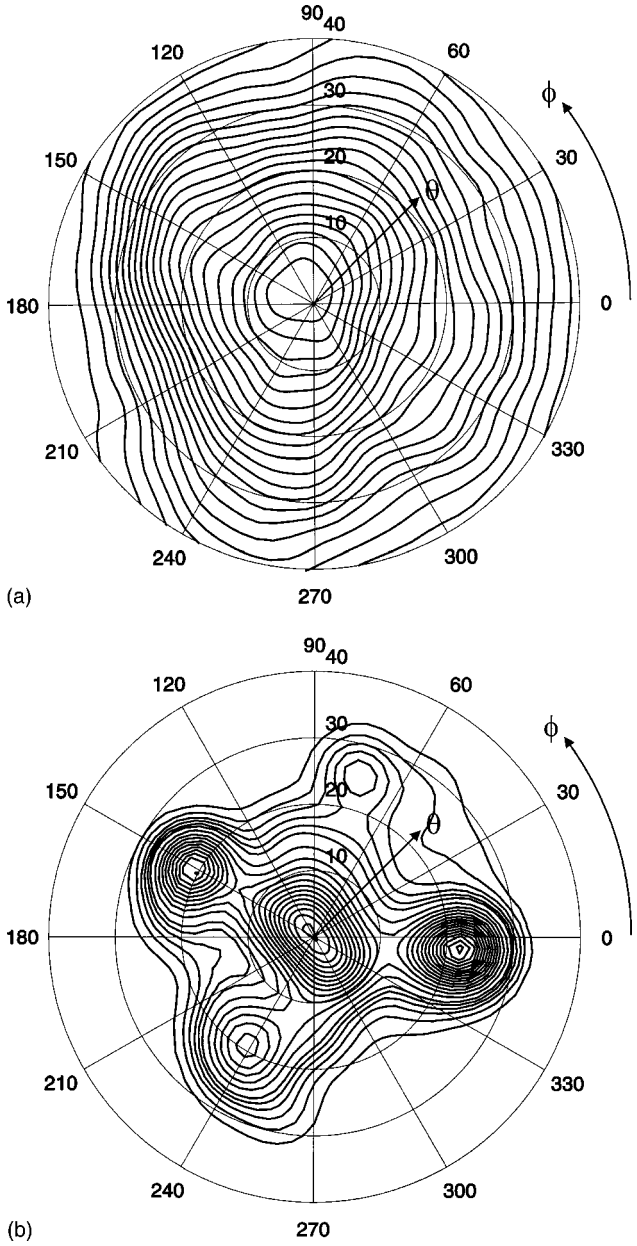

FIG. 4. (a) RHT of the image shown in Fig. 3 (only 200$\times$200 pixels in the center of the upper half of the image around the larger precipitate was selected) obtained by using a Savitsky–Golay filter with a length of 3 pixels for the determination of the local slopes in the image. No peaks corresponding to facets can be detected in the RHT. (b) Analogous RHT as in a but now for a filter length of 25 instead of 3 pixels. For each 90 °ϕ (azimuth) a peak at about 22 °θ. (inclination) can be readily discerned in the RHT corresponding to facets near to MnO{227}.

C. Dissolved MnO precipitates

Dissolution of only the MnO precipitates without affecting the Cu in combination with the supposition that the facets of the precipitate correspond to {111}MnO//{111}Cu would result in sharply defined faceted etch pits which could be nicely used to test the performance of the RHT. In Fig. 5, a SFM image shows three etch pits obtained by dissolving precipitates probably without much affecting the Cu. All the three etch pits show similar faceting. From this image an area of 100$\times$100 pixels is selected for the RHT. The RHTs for Savitsky–Golay filter lengths of 3 and 13 pixels are presented in Figs. 6(a) and 6(b), respectively. The RHT for a filter length of 13 pixels shows four peaks corresponding to four probably {111} facets. For a filter length of 3 pixels the results are not as dramatically poor as for the ones shown in Fig. 4(a), but also in this case the four facets are less-well resolved and one is not revealed at all. The results of the DFOD are given in Table III.

As in Figs. 1 and 3 the four facets have about the same polar angle θ and occur with a mutual ϕ-angle difference of about 90° and thus the surface normal is close to [001]. In the DFOD one facet is clearly out of line and shows the largest error and in fact corresponds to the facet which is not revealed in the RHT obtained with a 3-pixels filter length. Since the expected facets are {111} the expected polar angle θ for the four facets in the case the surface normal is one along the $\langle 100 \rangle$ direction is 54.7°. The four facets observed are indeed in fair correspondence with {111} facets. One of the clear facets with $\theta \approx 60°$ (at $\phi \approx 170°$) and another one

TABLE II. Orientation and deviation using spherical coordinates in degrees of the facets of the MnO precipitate protruding out of the Cu surface as shown in the upper part of Fig. 3 as obtained by the DFOD.

	Facet 1	Facet 2	Facet 3	Facet 4
Azimuth ϕ	−119.3	−4.6	70.4	150.3
$d\phi$	3.4	0.9	4.9	2.0
Inclination θ	20.6	23.1	21.9	21.3
$d\theta$	0.9	1.0	1.6	0.8

with $\theta \approx 50°$ (at $\phi = 355°$) having a mutual ϕ-angle difference of about 180° indicate a 5° tilt with respect to the ⟨100⟩ surface normal. At these high θ values the possibility that tip convolution effects which are in fact dilation effects[14,8,10,26,27] arise are substantial, although the present results can be explained without tip dilation. In principle this is possible, because the pyramidal tip used has a half angle of 35.3° (over the side faces of the pyramid) which allows measurements up to a θ angle of 54.7°. However, due to tilt of the tip (the cantilever makes and an angle of about 11° with the substrate surface) the maximum measurable angle for scanning in the direction during which the measurement is performed becomes about 65°.[28]

D. MnO precipitates viewed along high-index directions

The earlier three examples correspond to images having as horizontal planes more or less cube planes of Cu and MnO. The circumference made by the intersection of the cube plane with the MnO octahedron is in that case also clear from a crystallographic point of view. If the ϕ and θ angles for the facets are obtained by RHTs or DFOD the crystallography of the facets can be determined relatively easy. However, the situation is not always that easy. In Fig. 7 the SFM images show nicely faceted MnO precipitates, however, their crystallographic orientation is not clear. Accurately obtained ϕ and θ angles of the facets can now not directly be translated into the crystallography of the facets.

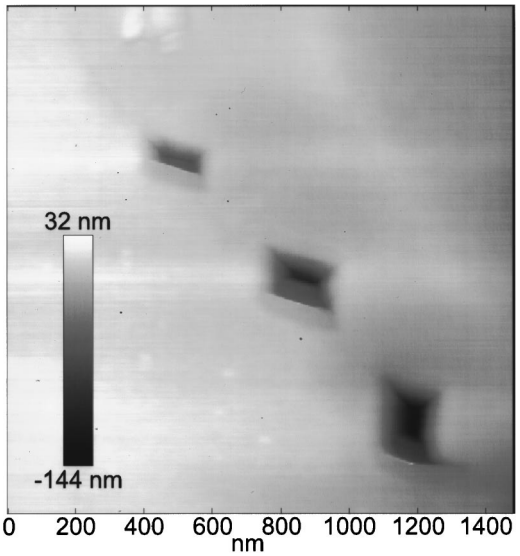

FIG. 5. Experimental SFM height image showing three etch pits in Cu as obtained by etching the MnO precipitates sticking out of the Cu surface. The faceting of the three etch pits is similar.

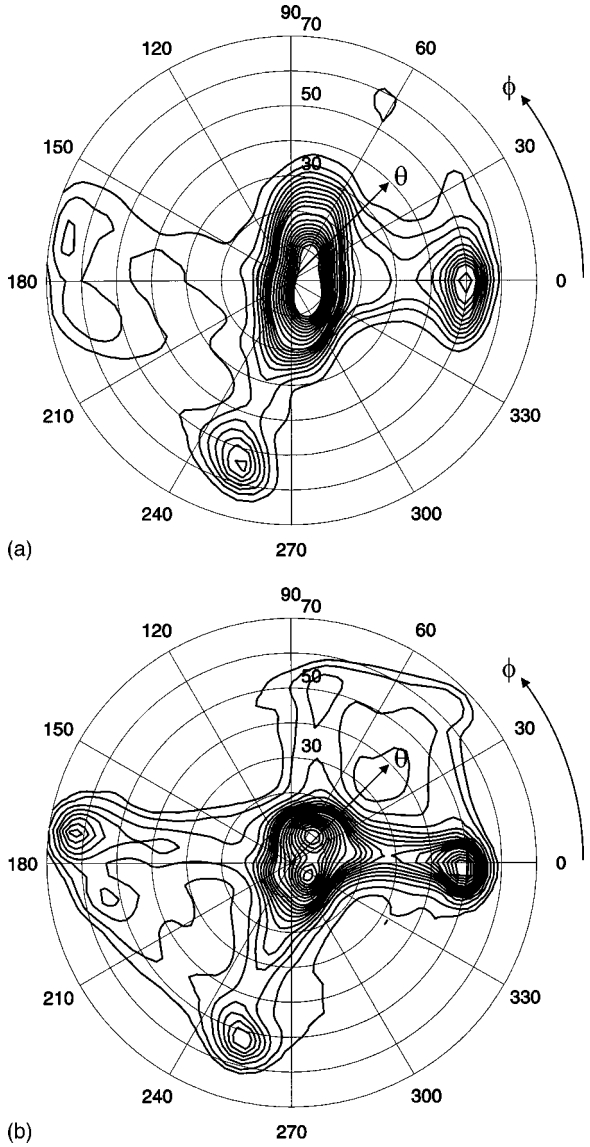

FIG. 6. (a) RHT of the image shown in Fig. 5 (only 200×200 pixels centred on the lowest left etch pitch) obtained by using a Savitsky–Golay filter with a length of 3 pixels for determining the local slopes in the image. Two clear facets and one faint facet can be detected at inclination angles θ of 50–60 °θ. (b) Analogous RHT as in (a) but now for a filter length of 13 instead of 3 pixels. Three clear facets and one faint facet can be detected at for each 90 °ϕ at 50–60 °θ. These four facets correspond well with the orientation of the expected {111} facets.

TABLE III. Orientation and deviation in orientation using spherical coordinates in degrees of the facets of the lowest left etch pit in Cu shown in Fig. 5 as obtained by the DFOD.

	Facet 1	Facet 2	Facet 3	Facet 4
Azimuth ϕ	−104.4	−2.7	57.5	174.6
$d\phi$	1.2	0.8	12.5	1.9
Inclination θ	53.8	50.0	33.0	60.8
$d\theta$	1.0	1.3	6.5	2.5

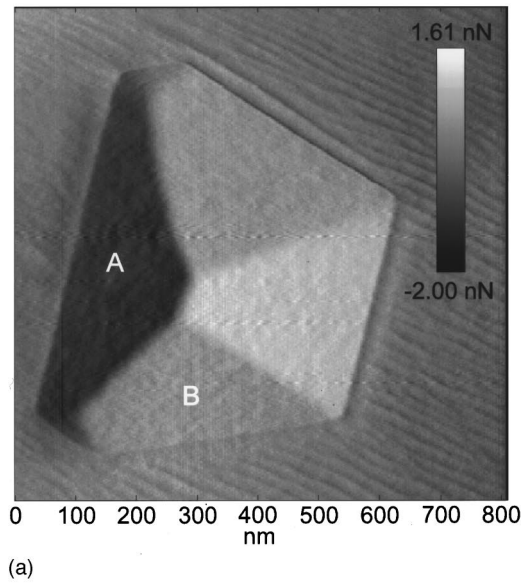

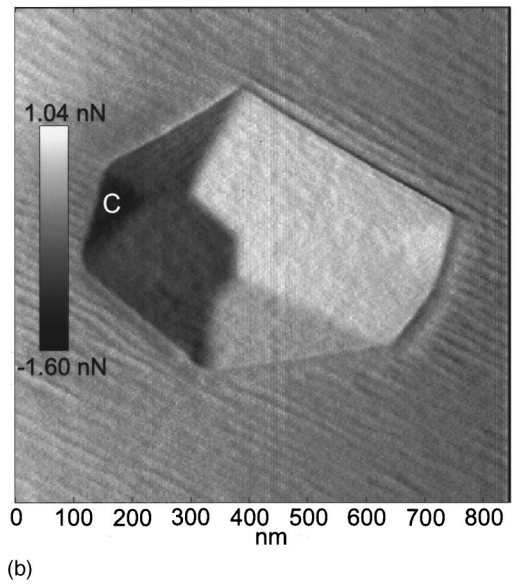

FIG. 7. Experimental SFM force images showing sharply faceted MnO precipitates protruding out of a Cu surface.

Still, since the precipitate shape is an octahedron, the circumference made by intersection of an arbitrary plane with the octahedron in principle reveals the normal of this plane and the crystallographic directions making the circumference. Since the different facets of the experimental octahedron do not always have equal area (i.e., the octahedron is not perfectly shaped but still solely consists of {111} planes), the only useful experimental parameters are the angles between the different directions within the circumference. A theoretical reproduction of these experimentally obtained angles reveals the orientation of the octahedron. The experimental circumference as shown in the 400×400 pixel image of Figs. 7(a) and 8(a) is reproduced theoretically with an accuracy of ±1 pixel in Fig. 8(b) for a normal of the surface plane around the precipitate corresponding to the $[0.58\ \pm0.02\ \ 0.27\pm0.01\ \ 1]$ direction. The crystallographic orientation of the precipitate is now fully fixed and as an example the orientations of two facets A and B indicated in Fig. 7(a)

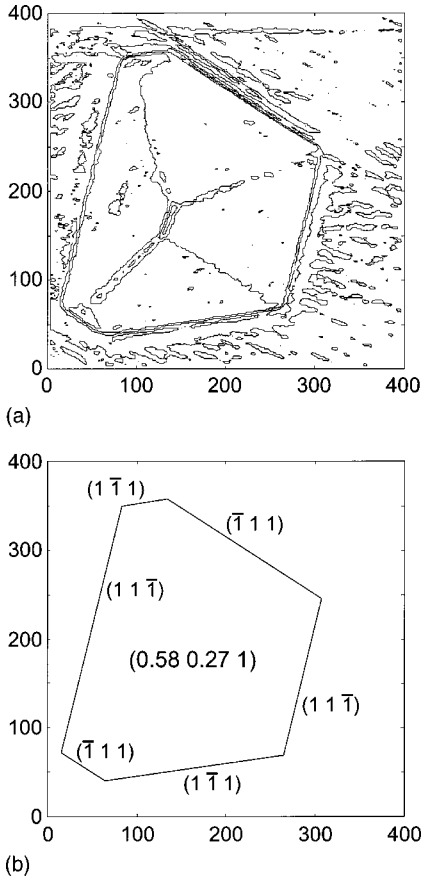

FIG. 8. (a) Contour image showing the local inclination-angle θ values of the image shown in Fig. 7(a) as obtained by a Savitsky–Golay filter with a length of 9 pixels. The circumference made by intersection of the MnO precipitate with the Cu surface is sharply defined in such an image. (b) Accurately reconstructed circumference based on the experimental circumference shown in Figs. 7(a) and 8(a). Angles between the directions in the experimental circumference are reproduced if the (0.58 0.27 1) plane is intersecting with the indicated {111} planes of the MnO octahedron present within the Cu.

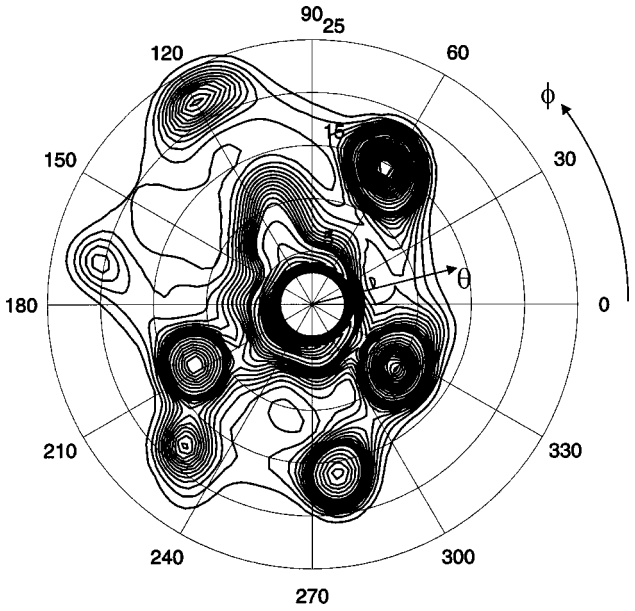

FIG. 9. RHT of the image shown in Fig. 7(b) obtained by a Savitsky–Golay filter with a length of 15 pixels. Seven facets observed in the image are well reproduced in the RHT indicating that Ar^+ ion milling of MnO precipitates in Cu at grazing angles of 14° followed by annealing in air at 130 °C produces facets with inclination angles in-between about 10 and 22°.

TABLE IV. Orientation and deviation using spherical coordinates in degrees of the facets of the MnO precipitate protruding out of the Cu surface as shown in Fig. 7(b) as obtained by the DFOD.

	Facet 1	Facet 2	Facet 3	Facet 4	Facet 5	Facet 6	Facet 7
Azimuth ϕ	−152.9	−131.4	−81.6	−37.2	61.5	121.1	169.8
$d\phi$	0.6	3.9	0.4	1.3	0.7	1.3	0.7
Inclination θ	12.3	17.7	16.1	9.9	14.7	22.2	20.9
$d\theta$	0.1	0.8	0.1	0.1	0.1	0.5	0.4

are determined as near to (8 5 7) and $(5\bar{1}7)$, respectively. The latter facet corresponds to a polar plane and therefore is probably not the real facet present. However, for high index planes minute changes in orientation make the difference between polar and nonpolar planes. Although very distinct and sharp facets are observed as illustrated by Fig. 7, their crystallography apparently does not have to correspond to low index planes.

As a final example of the ability of the RHT with Savitsky–Golay differentiation filters with variable length, the RHT of the SFM image shown in Fig. 7(b) using a 15-points filter is given in Fig. 9. Seven facets are clearly revealed by the RHT for grazing inclination angles ranging from about 10 to 22 °θ. Even the small facet indicated by C in Fig. 7(b) is still revealed by the RHT at about 170 °ϕ and 20 °θ. The results of the DFOD are give in Table IV and indicate that for relatively accurate images such as shown in Fig. 7 (but then the corresponding height image) the determination of the orientation of facets can occur readily with an accuracy of 1° in azimuth ϕ and 0.1° in inclination ϕ. Finally, the observations make clear that Ar^+ ion milling of MnO precipitates in Cu at grazing angles of 14° followed by annealing in air at 130 °C produces clear facets with inclination angles in-between about 10° and 22°.

V. CONCLUSIONS

Two tools for the analyses of facets in SPM images were described and to illustrate their usefulness were applied to MnO precipitates protruding out of a Cu surface. The first approach is an adaptation of the RHT proposed in Ref. 4 by implementing Savitsky–Golay filters with variable filter lengths for the determination of all the local slopes in a SPM image. This variable filter length is shown to be useful for detection and analyses of corrugations with different length scales in a SPM image and appeared quite essential to improve the detectability of facets in the presence of noise in the image. The second tool allows the direct quantitative determination of the orientation of facets in SPM images. It also employs Savitsky–Golay filters.

MnO precipitates in Cu as obtained by internal oxidation have octahedral shapes owing to a termination by eight polar {111} planes parallel to the eight Cu{111} planes. Ion milling the Cu sample with dispersed MnO precipitates at grazing angles of 14° followed by annealing at 130 °C in air results in sharply faceted precipitates protruding out of relatively flat Cu surfaces. The facets have an inclination of typically 10–20° and are nonpolar and generally not of low-index type despite their sharp faceting. Preferentially etching the MnO precipitates revealed etch pits bound by {111}Cu planes as expected and further demonstrated the potential importance of the RHT and DFOD.

ACKNOWLEDGMENTS

The research described in this article is supported by the foundation for technical sciences (STW) and the foundation for fundamental research on matter (FOM-Utrecht). Discussions with Dr. Jacob Kerssemakers are gratefully acknowledged.

[1] J. Krim and G. Palasantzas, Int. J. Mod. Phys. B **9**, 599 (1995).
[2] J. H. Jeffries, J.-K. Zuo, and M. M. Graig, Phys. Rev. Lett. **76**, 4931 (1996).
[3] H.-N. Yang, G.-C. Wang, and T.-M. Lu, Phys. Rev. Lett. **73**, 2348 (1994).
[4] M. Li, G.-C. Wang, and H.-G. Min, J. Appl. Phys. **83**, 5313 (1998).
[5] K. Carneiro, C. P. Jensen, J. F. Jorgensen, and J. Garnoes, Ann. CIRP **44**, 381 (1995).
[6] M. C. Salvadori, M. G. Silveira, and M. Cattani, Phys. Rev. E **58**, 6814 (1998).
[7] P. Daguier, S. Henaux, E. Bouchaud, and F. Creuzet, Phys. Rev. E **53**, 5637 (1996).
[8] J. Aué and J. Th. M. De Hosson, Appl. Phys. Lett. **71**, 1347 (1997).
[9] A. C. Hillier and M. D. Ward, Science **263**, 1261 (1994).
[10] A. Schwarz, U. D. Schwarz, H. Bluhm, and R. Wiesendanger, Surf. Interface Anal. **23**, 409 (1995).
[11] A. Asenjo, J. Gómez-Herrero, and A. M. Baró, J. Microsc. **188**, 243 (1997).
[12] T. Inoue, Y. Yamamoto, M. Satoh, A. Ide, and S. Katsumata, Thin Solid Films **281–282**, 24 (1996).
[13] C.-H. Nien and T. E. Madey, Surf. Sci. **380**, L527 (1997).
[14] D. Schleef, D. M. Scheafer, R. P. Andres, and R. Reifenberger, Phys. Rev. B **55**, 2535 (1997).
[15] A. Savitsky and M. J. E. Golay, Anal. Chem. **36**, 1627 (1964).
[16] F. Ernst, Mater. Res. Soc. Symp. Proc. **183**, 49 (1990).
[17] B. J. Kooi, H. B. Groen, and J. Th. M. De Hosson, Acta Mater. **46**, 111 (1998).
[18] B. J. Kooi and J. Th. M. De Hosson, Acta Mater. **46**, 1909 (1998).
[19] K. L. Merkle, Ultramicroscopy **37**, 130 (1991).
[20] W. Mader, Z. Metallkd. **83**, 478 (1992).
[21] W. P. Vellinga and J. Th. M. De Hosson, Acta Mater. **45**, 933 (1997).
[22] P. W. Tasker, J. Phys. C **12**, 4977 (1979).
[23] D. M. Duffy, J. H. Harding, and A. M. Stoneham, Philos. Mag. A **67**, 865 (1993).
[24] M. W. Finnis, J. Phys.: Condens. Matter **8**, 5811 (1996).
[25] F. N. Rhines, Trans. Metall. Soc. AIME **137**, 246 (1940); F. N. Rhines, W. A. Johnson, and W. A. Anderson, *ibid.* **147**, 205 (1942).
[26] J. S. Villarrubia, Surf. Sci. **321**, 287 (1994).
[27] U. D. Schwarz, H. Haefke, P. Reimann, and H.-J. Güntherodt, J. Microsc. **173**, 183 (1994).
[28] MultiMode SPM Instruction Manual, Version 4.31ce, 1996–1997, Digital Instruments, Santa Barbara, CA.